Proceedings of the Seventh International Conference on
Railway Technology: Research, Development and Maintenance
Edited by: J. Pombo
Civil-Comp Conferences, Volume 15, Paper 6.14
Civil-Comp Press, Edinburgh, United Kingdom, 2026
ISSN: 2753-3239, doi: 10.4203/ccc.15.6.14

Field-Calibrated MBS Model for Simulation of Railway Switch Actuation with a Trapped Foreign Object

S. K. K. Bysani, B. A. Pålsson and E. Kabo

Department of Mechanical Engineering/CHARMEC, Chalmers University of Technology, Gothenburg, Sweden

Abstract

Railway switches are critical for network flexibility but remain a significant source of operational disruptions, particularly when foreign objects become trapped between the switch and stock rails during actuation. Such obstructions can prevent proper switch closure, causing delays and increased maintenance costs, or, in cases of local gauge narrowing, raise the risk of derailment if undetected. It is therefore of interest to detect such disturbances as efficiently as possible. This study explores whether switch rail end position detection can be achieved using drive output alone, without supplementary sensors that require additional systems and maintenance. When an obstruction is present, the drive must exert additional force to close the induced gap, altering its force and current profile in a way that may indirectly reveal the presence of a foreign object. To better quantify this influence and allow for future development of detection algorithms, a multi-body system (MBS) model of switch actuation under a trapped foreign object is developed and calibrated against field measurements of forces in actuation rods and foreign object. After calibration of the slide chair friction coefficient and drive stiffnesses, the simulated results show good agreement to field measurement

results. The model therefore provides a foundation for combining simulation and field data to develop an efficient detection method for foreign objects.

Keywords: railway switch, point machine, trapped foreign object, field measurement, multibody dynamics simulation, model calibration

1 Introduction

Switches and crossings (S&Cs) are integral to modern railway infrastructure, providing the network flexibility required to route trains between different tracks [1,2]. However, this critical functionality comes with a substantial operational burden; because S&Cs contain complex moving parts, they are susceptible to mechanical faults that trigger traffic disruptions and significant maintenance. Consequently, the unreliability of a single switch can propagate delays across the railway network [3].

An important contributor of switch faults is the intrusion of foreign objects such as ballast stones, metal debris, snow, or ice etc, lodged between the switch rail and the stock rail during actuation [4, 5]. According to data from the Swedish Transport Administration (Trafikverket), approximately 14% (1,188 out of 8,597) of all recorded switch faults in 2017 were caused by trapped foreign objects, predominately ice and snow. Detailed classifications of these failure modes are documented in [6, 7].

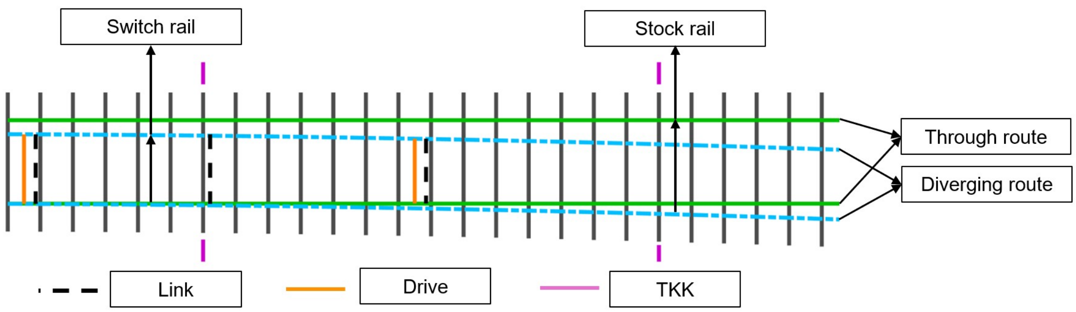

Figure 1: Schematic top view of the studied switch panel in a UIC60-760-1:15 S&C setting [6].

In standard Swedish S&C designs, the task of detecting these obstructions relies on a combination of electromechanical drives (point machines) and specialized end position sensors known as Tungkontrollkontakt (TKK, or switch rail control contacts) [5, 8, 9], as illustrated in Figure 1 (see [6, 7] for detailed design specifications). The number of drives and TKK pairs vary with the size of the S&C. The TKK reports a fault (not in control) if the gap between switch and stock rail reaches or exceeds a maximum of 13 mm [10]. The physical actuation of the switch rail between the through route and the diverging route is driven by two drives, each capable of exerting a maximum force of 6 kN [10, 11]. The drives maintain control and confirm locking only if the rail gap at the drive location is less than a maximum of 5 mm [10]. A critical vulnerability of this framework is the reliability of the locking detection mechanism and the TKK sensors themselves that require timely maintenance and adjustment.

To address these limitations, a non-intrusive approach can be derived from the mechanics of the obstruction itself. When a switch rail encounters a trapped foreign object during actuation, the drives must exert additional force to overcome the localized resistance in an attempt to close the gap within acceptable tolerances by bending the switch rail around the object. This mechanical resistance directly alters the force and electrical current profiles of the drives. By characterizing these variations against a nominal baseline, an end position detection system can be developed to identify trapped objects or emerging faults by analyzing drive outputs.

To better understand the magnitude of these variations as a function of foreign object location, size and operational conditions, this paper develops a multibody simulation model of a switch panel with actuation that is calibrated to field measurements. This model can then be applied for development of object detection algorithms.

The remainder of this paper is organized as follows. First, a detailed overview of the measurement campaign with some example results is provided. Next, the MBS model of the switch actuation is described followed by the model calibration w.r.t friction coefficient between bottom of the switch rail and slide chair and individual drive stiffnesses. This is followed by a conclusion which summarizes the key contributions and sheds light on future work.

2 Field measurements

A two-day measurement campaign was conducted at Trafikverksskolan in Ängelholm, Sweden, on 3–4 November 2025. The tests were performed on a UIC 60-760-1:15 S&C assembly that is dedicated to the training of track engineers. The S&C is actuated by two JEA 73 drives, each consisting of an electric motor coupled to a gear mechanism that provides the required mechanical actuation as can be seen in Figure 2. Before starting the measurement campaign, the clutch of the motors are adjusted to slip at 2 A of current.

An overview of the instrumented switch setup can be seen in Figure 2. The setup consisted of:

1. Drive rod force measurements: The drive rods connecting the drive motor to the switch rail are equipped with strain gauges to measure bending-induced strain which is converted into actuation force. A free-body diagram of an instrumented drive rod is shown in Figure 3. The drive rod is connected to the switch rail at point A and to the drive motor at point B. Due to eccentricity in the attachment geometry and applied loading, the region of the drive rod immediately below the attachment point experiences the maximum bending moment (under the assumption that $M_2 = 0$) as seen in Figure 3. Strain gauges are therefore installed at this location to capture the peak bending response of the rod. Four gauges were installed (two gauges in a T-configuration on top and bottom of the

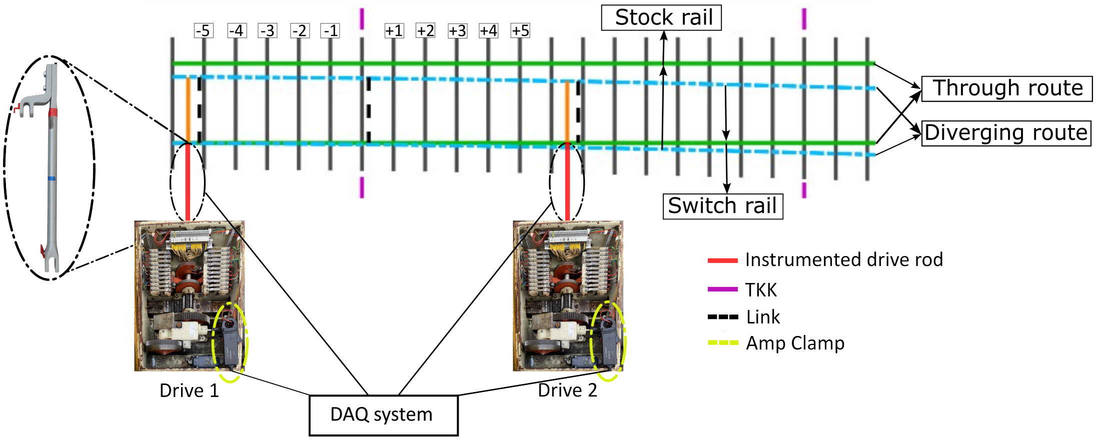

Figure 2: Overview of the instrumented switch setup consisting of drive rods and amp clamps connected to the data acquisition (DAQ) system. The numbers indicate sleeper number w.r.t the first set of TKKs.

rod) and configured in a Wheatstone bridge for a single bending strain output. The lateral switch rail actuation force $R_{1\mathrm{H}}$ was then estimated from the bending strain via the bending moment and knowledge of the height offset h between the instrumented section and the switch rail connection at point 1.

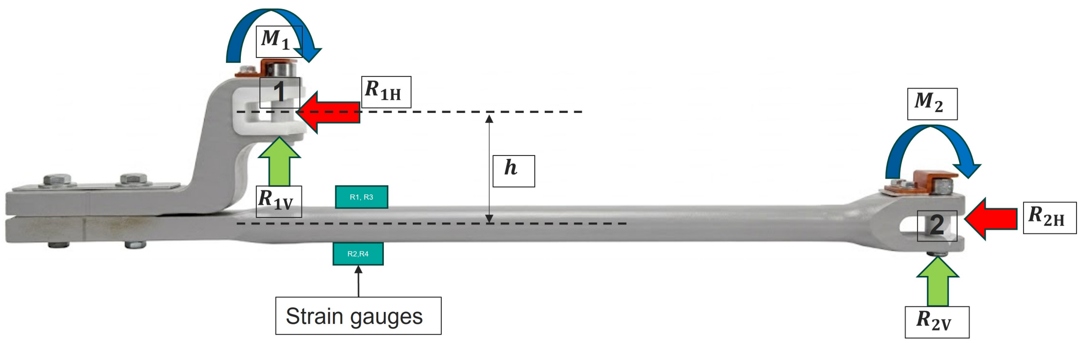

Figure 3: Free Body Diagram of the drive rod attached between the switch rail and the motor

2. Drive current measurements: The JEA 73 drives are powered by DC motors. Variations in motor current associated with the presence of trapped foreign objects were measured using non-intrusive Hall-compensated current clamps supplied by Dewesoft. The clamps have a measurement range of 30 A (AC or DC peak) and a sensitivity of 100 mV/A. The amp clamps connected to the data acquisition system (DAQ) can be seen in Figure 2. The current clamps were factory-calibrated.

3. Force measurements on the foreign object: The compressive force exerted by the drive on a foreign object trapped between the switch rail and the stock rail was measured using a force load cell adapted to replicate the geometry and

placement of a representative foreign object. The load cell has a sensitivity of 1 mV/V and a nominal capacity of 20 kN, as shown in Figure 4a. The height of the load cell is 13 mm. To mount the load cell onto the inclined surface of the switch rail, custom rigs (as seen in Figure 4b) were fabricated using additive manufacturing.

(a)

(b)

Figure 4: (a) Force load cell used in the measurements. (b) Square rig to hold the load cell. Additional spacers can be added to the rear of the load cell

A Dewesoft Sirius modular DAQ system, with a capacity to record 8 channels simultaneously was used in these measurements. In total 5 channels i.e. strains from drive rods 1 and 2, current in drives 1 and 2, and force from the load cell were measured at a fixed sampling frequency of 1 kHz.

Prior to the measurement campaign, the drives were tuned to operate under standard operating conditions. The main measurement campaign consisted of tests conducted at all eleven sleeper locations between the two drives as can be seen in Figure 2. At each location, foreign objects of increasing sizes (0, 5, 10, 13, 16, 18, 21, 23, 26, 29, and 31 mm) were introduced. The foreign objects were represented by spacers and/or load cell with the load cell present for all objects 13 mm and larger. The foreign object size was incremented stepwise until one of the drives experienced slip, defined as a failure to lock and thereby not being in control.

Raw measurement data were filtered using a moving-average filter with a 0.1 second window to reduce high-frequency noise and smoothen the signals for subsequent analysis. The filtering parameters were selected to reduce measurement noise without affecting the timing, magnitude, or qualitative trends of the measured responses. An example of the resulting time histories for all measured quantities, corresponding to the case where the object is located at the first TKK (refer to Figure 2), is shown in Figure 5.

The results show that all measured quantities exhibit an increasing response with increasing object size. Relative to the baseline case without a foreign object (0 mm), the change associated with an object size of 5 mm is not distinguishable in any of

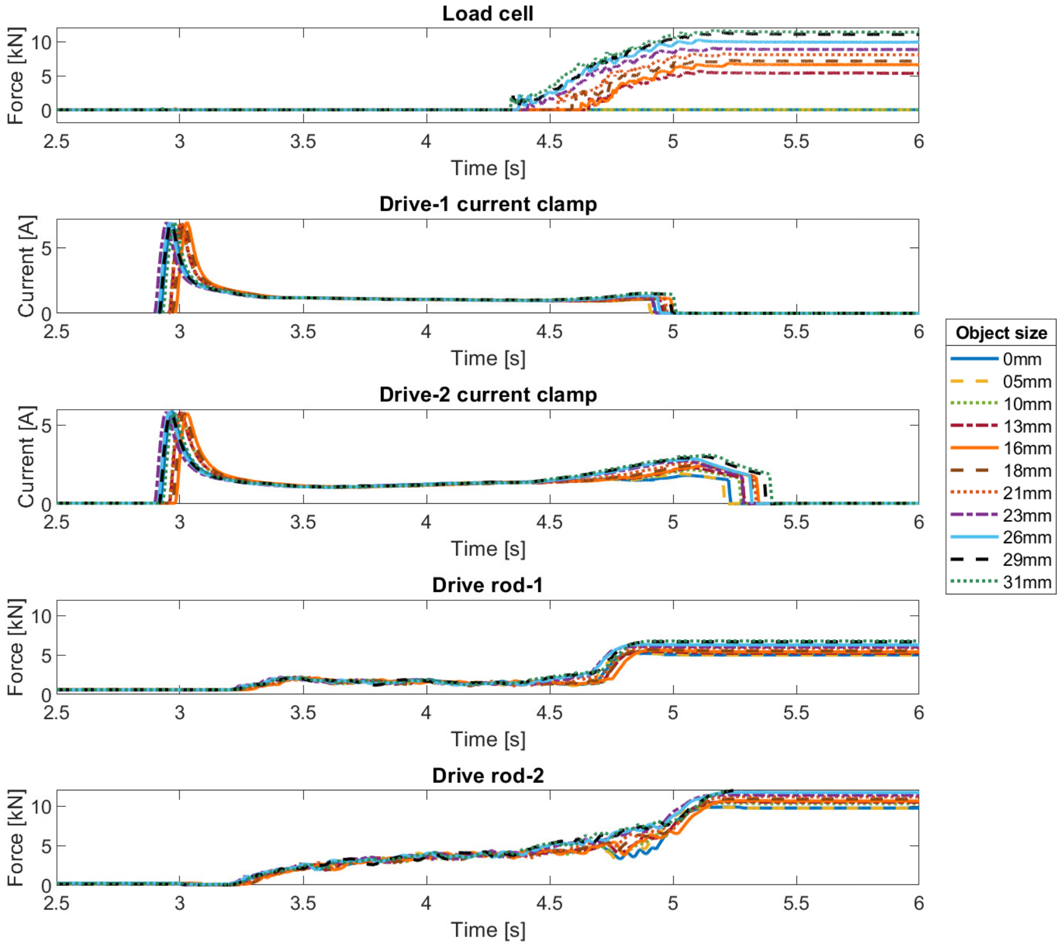

Figure 5: Time histories of load cell force, clamp currents (Drive 1 and Drive 2), and drive-rod forces for varying object sizes (0–31 mm) located on sleeper 6 (location of the first TKK). Load cell results only available for objects 13 mm and larger.

the measured signals. In contrast, for object sizes of approximately 10 mm and 13 mm, both the current and force responses from Drive 2, are clearly distinguishable and display regions of increased magnitude, reflecting the higher resistance induced by the foreign object. Drive 2 delivers more force than expected as a worn clutch made it difficult to tune the force level. This is a result of the switch not being maintained to track standard as it is solely employed for educational purposes.

3 Multibody simulation model

MBS of switching operations were carried out in Simpack [12]. Rails are modelled as flexible bodies from Timoshenko beam elements using the non-linear flextrack module. The varying properties of the switch rails due to their tapered ends are accounted for [13]. All rails are condensed into super elements using a Craig-Bampton reduction [14]. Sleepers are omitted to reduce computational demands, given the quasi-static nature of the switching operation as dynamic wheel loads are excluded. Each drive is modelled as a moving marker under displacement control, actuating the switch rail through a bi-linear bushing connection. The corresponding force–displacement curve comprises two regions: an initial linear increase in force until a saturation level is reached, beyond which the stiffness is near-zero. This near-zero stiffness in the second region is retained for numerical stability, ensuring the integrator remains well-conditioned during simulation. The stiffness of the initial linear region is calibrated against field measurements, as is the friction coefficient between the bottom of the switch rail and the slide chair.

The foreign object is modelled as a bi-linear spring, with a linear stiffness of 40 kN/mm upon contact and inactive otherwise. A detailed description of the switch modelling framework adopted in this study is provided in [6]. The topology of the MBS model used can be seen in Figure 6.

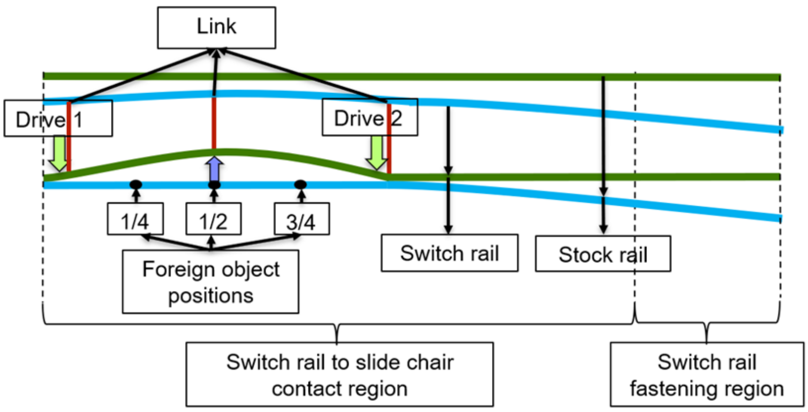

Figure 6: Topology of the MBS model illustrating the different parts as well as support condition regions (slide chair or fastening) for the switch rails (refer to [6]). The switch rail deformation pattern when a foreign object is placed at the halfway position between the drives is indicated.

The procedure for simulating drive responses in the presence of a trapped foreign object follows four sequential steps [15]. First, the model is brought to static equilibrium. A full switching cycle is then simulated by actuating the drives under displacement control, transitioning from the through route to the diverging route and back. The time–displacement function governing this actuation is illustrated in Figure 7. At the onset of the return movement to the through route, a foreign object is introduced. The foreign object becomes active once the gap between the switch rail and stock rail reduces to the size of the foreign object. It is to be noted that Drive 2 requires an additional 0.2 s to complete the return movement of the actuation to match the measured response.

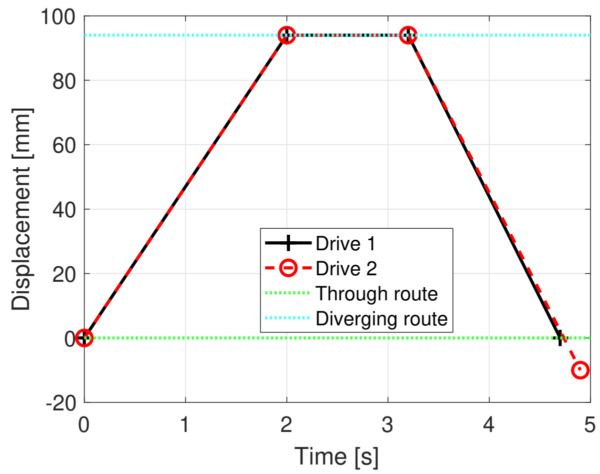

Figure 7: Time-displacement function governing the actuation of the respective drive moved markers.

4 Model calibration

Model calibration is performed using force measurements obtained from drive rods and load cell. Current measurements are excluded from this process, as the drives within the simulation model are represented as simplified moved markers rather than fully characterised mechanical assemblies.

4.1 Friction coefficient

First, the friction coefficient between the bottom of the switch rail and slide chair is calibrated with force measurements when there isn't any trapped foreign object. The friction coefficient is varied from 0.1 to 0.5 and the comparison of the responses from both the drives are as shown in Figure 8. A friction coefficient of 0.4 gives the best fit to field measurement results for both drives.

4.2 Drive stiffness

The stiffness of each drive was calibrated individually against field measurements by introducing a 13 mm foreign object at the respective drive location. In doing so the force response in the load cell is more or less decoupled from the influence of the other drive in each test.

Drive stiffness calibration is performed through a manual grid search, with values of 750 and 810 kN/m identified as the best fit to field measurements for Drive 1 and Drive 2, respectively. To illustrate the influence of drive stiffness, Drive 1 was evaluated across stiffness values of 75, 750, and 7500 kN/m (the calibrated stiffness and weak and stiff extremes) while the stiffness of Drive 2 was held constant at the cali-

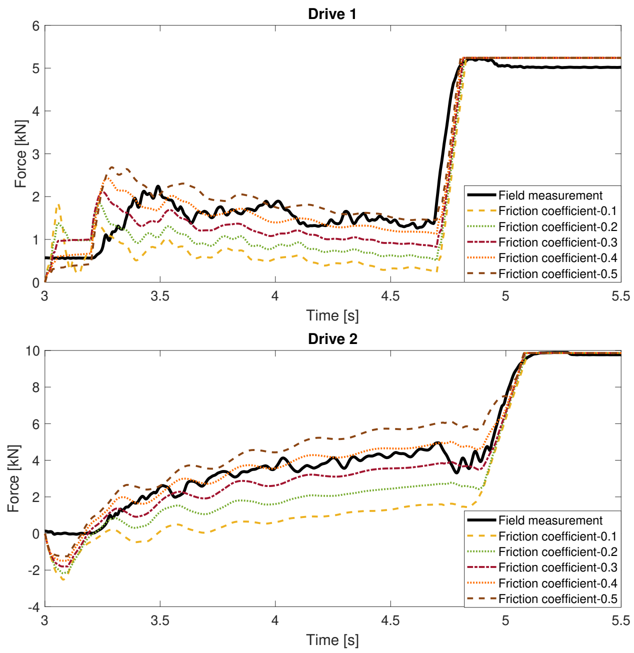

Figure 8: Calibration of friction coefficient between bottom of switch rail and slide chair against field measurements without any trapped foreign object

brated value; the resulting comparison with field measurements is shown in Figure 9. Following the same approach, the influence of Drive 2 stiffness is subsequently illustrated by varying its stiffness across 81, 810, and 8100 kN/m with as shown in Figure 10.

Comparative analysis demonstrates that the medium stiffness level yields the closest agreement with the field measurement across all evaluated physical quantities. Under the low stiffness configuration for Drive 2, the simulated switch rail displacement lagged significantly behind its corresponding moving marker. Consequently, the residual gap at the end of the actuation cycle reached approximately 26 mm, preventing the switch rail from making physical contact with the 13 mm foreign object.

The calibrated drive model is validated by simulating the responses when foreign objects of 13 mm and 29 mm are placed at the sleeper position close to the TKK — and comparing predicted drive forces and foreign object towards field measurement results, as shown in Figure 11. For Drive 1, both the point of contact with the foreign object and the subsequent force build-up through to saturation show good agreement with the measured data across both object sizes. Drive 2 presents a slightly less consistent picture: while the predicted contact point aligns reasonably well with field measurements, the post-contact force build-up exhibits a stiffer response in the MBS model than observed in practice. The compressive force developed within the foreign object, however, shows close agreement in both cases, with near-identical rates of increase up to saturation. Overall, this comparison demonstrates that the calibrated MBS model is capable of capturing the key nonlinear response characteristics across all three measured quantities to a reasonable degree.

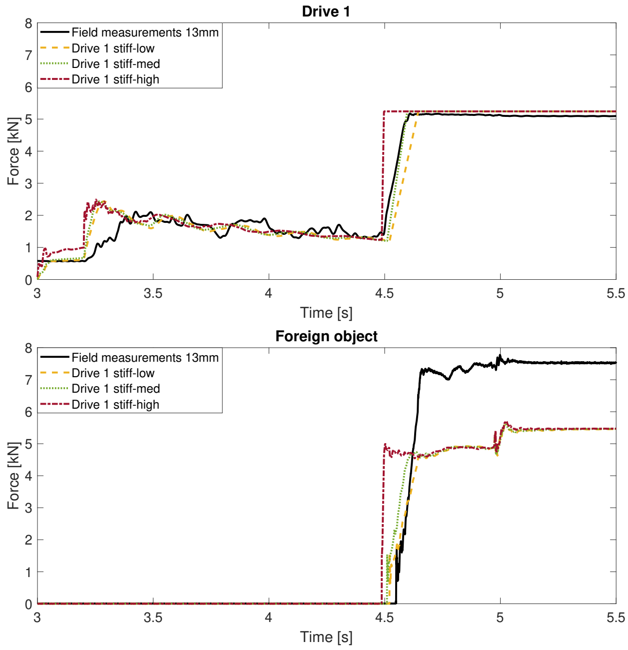

Figure 9: Comparison of simulated drive responses and force on foreign object, across three stiffness levels (low, medium, and high) against field measurements for Drive 1, with a 13 mm foreign object positioned at Drive 1.

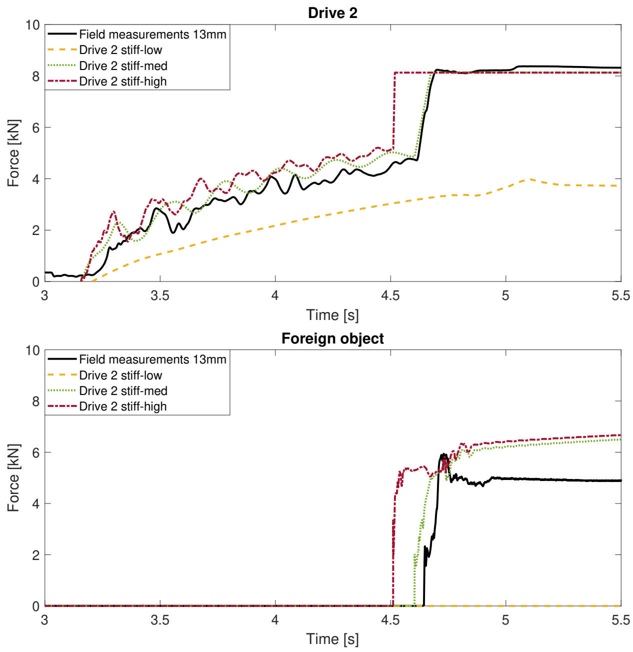

Figure 10: Comparison of simulated drive responses and force on foreign object, across three stiffness levels (low, medium, and high) against field measurements for Drive 2, with a 13 mm foreign object positioned at Drive 2.

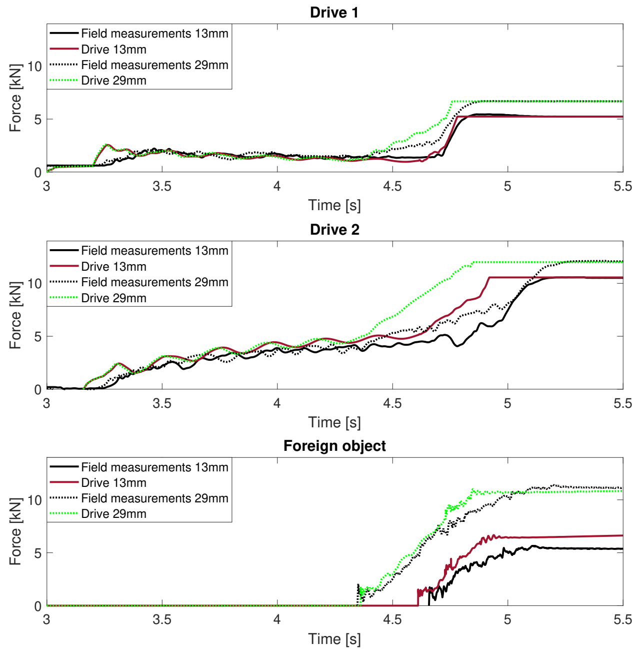

Figure 11: Comparison of simulated drive responses and force on foreign object after calibration for two object sizes (13 and 29mm) against field measurements when the foreign object is placed at the TKK

5 Concluding remarks

This paper presented the calibration of an MBS model of railway switch actuation in the presence of a trapped foreign object, validated against field measurements. A dedicated measurement campaign was conducted to record current and force responses from the drives and the foreign object, providing the reference data necessary for calibration. The MBS model, implemented in Simpack, was calibrated in a sequential manner. First, the friction coefficient between the switch rail base and slide chair was calibrated, with a value of 0.4 yielding the best agreement with field measurements. The stiffness of each individual drive was subsequently calibrated against force measurements recorded with a foreign object positioned at the respective drive. Stiffness values of 750 kN/m for Drive 1 and 810 kN/m for Drive 2 produced the closest agreement with the field measurement data. The calibrated model was then validated by simulating the switch response for two foreign object sizes placed at the TKK location, demonstrating good agreement across all three measured quantities.

Future work will focus on leveraging the calibrated model to generate simulated responses across diverse operational conditions, forming the basis for developing and validating a robust, real-world foreign object detection method.

Acknowledgements

The current work is part of the activities within the Centre of Excellence CHARMEC (CHAlmers Railway MEChanics, www.chalmers.se/charmec). The work is mainly funded by Trafikverket (Swedish transport administration) under contract number 2021/53614 and partly by Project 101102001-FP2 - R2DATO in Europe's Rail and Horizon Europe.

References

[1] Johansson A, Pålsson B, Ekh M, Nielsen J C, Ander M K, Brouzoulis J and Kassa E (2011) Simulation of wheel–rail contact and damage in switches & crossings. Wear 271(1-2), pp.472–481. doi: 10.1016/j.wear.2010.10.014.

[2] Pålsson B (2014) Optimization of railway switches and crossings. Doctoral thesis. Chalmers University of Technology, Department of Mechanics and Maritime Sciences, Gothenburg, Sweden.

[3] Dutta S, Harrison T, Ward C P, Dixon R and Scott T (2020) A new approach to railway track switch actuation: Dynamic simulation and control of a self-adjusting switch. Proceedings of the Institution of Mechanical Engineers, Part F: Journal of Rail and Rapid Transit, 234(7), pp. 779–790. doi: 10.1177/0954409719868129.

[4] Paulsson B and Ekberg A (2022) More robust switches through improved control of the switch rail. Chalmers University of Technology, Department of Mechanics and Maritime Sciences, Research report 2022:01

[5] Blomqvist M and Blomqvist M (2013) The problems with railway switches-Proposals for future action. Bachelor thesis, KTH Royal University of Technology [in Swedish], 68 pp.

[6] Bysani S K K, Pålsson B A and Kabo E (2025) Multibody simulation of derailment risk in railway switches due to gauge narrowing caused by foreign objects. Vehicle System Dynamics, pp. 1–24. doi:10.1080/00423114.2025.2495227.

[7] Bysani S K K (2024) Influence of foreign objects on derailment risks in railway switches. Licentiate thesis, Chalmers University of Technology, 29 pp.

[8] Trafikverket (2021) Spårväxel. Requirements, TRVINFRA-00017 [in Swedish]

[9] Andersson R and Nilsson T (2015) The problems surrounding Easyswitch and the 60E switch standard. Master thesis, Lund University, Lund, Sweden, [in Swedish], 96 pp.

[10] Trafikverket (2022) Säkerhetsbesiktning av fasta järnvägsanläggningar. TDOK 2014:0240 [in Swedish], 155 pp

[11] Andersson D, Carlvik F, Kronvall-Bjelkengren F, Vamling O (2018) Risk analysis for rail transport–a study on the possibility of improvements for TKK and load imbalance based on risk analysis. Bachelor thesis, Chalmers University of Technology, MMSX20-18-27 report 2018:25, 90 pp.

[12] Simpack. Version 2022x.4: Dassault Systemes; (2022). Available from www.3ds.com

[13] Pålsson B A, Ambur R,Sebes M,Wang P,Shih J Y et.al (2023) A Comparison of Track Model Formulations for Simulation of Dynamic Vehicle–Track Interaction in Switches and Crossings. Vehicle System Dynamics, 61(3):698–724. https://doi.org/10.1080/00423114.2021.1983183.

[14] Craig R R and Bampton M C C (1968) Coupling of Substructures for Dynamic Analyses. AIAA Journal, 6(7):1313–1319.

[15] Bysani S, Pålsson B, Kabo E and Ekberg A (2025) Identification of trapped foreign object in railway switches using drive outputs. Proceedings of the 15th International Workshop on Structural Health Monitoring, California, USA, 9-11 September 2025.